CFD analysis of the NEXST-1 using JAXA's code

Hiroaki ISHIKAWA*, Dongyoun KWAK† and Zhong LEI†

* *Sanko Soft Co.ltd, 2-14-2-1106, Takadanobaba, Sinjuku, Tokyo, 169-0075, Japan*

† *Japan Aerospace Exploration Agency, 6-13-1, Osawa, Mitaka, Tokyo, 181-0015, Japan*

A flight test of a supersonic experimental airplane (NEXST-1) was conducted successfully by JAXA in October 2005. In this study some aerodynamics design concepts were verified by comparing the flight test results with CFD analysis using JAXA's CFD codes, a structured mesh code UPACS and an unstructured mesh code TAS. After the CFD codes was verified using a wind tunnel test results, the CFD results were compared with the flight test results. The aeroelastic deformation and the boundary layer transition data of flight test were taken into account to improve CFD analysis. The effect of the design concept of the NEXT-1 was also confirmed by CFD analysis.

1. Introduction

Flight test on a supersonic experimental airplane (NEXST-1 : National Experimental Super sonic Transport)[1] was conducted successfully by JAXA (Japan Exploration Agency) in October 2005 at Woomera test range, Australia[2]. (Figure 1) A lot of aerodynamic data were obtained on the flight test[3] to validate the design technology[4]. As shown Figure 2, four design concepts, arrow wing planform, warp of wing, area-rule body, and natural laminar flow wing were applied to the NEXST-1 to improve aerodynamic performance at supersonic cruise condition (lift coefficient, C_L=0.1 and Mach number, M_{inf}=2.0). In this study the four aerodynamics design concepts[5] were verified by comparing the flight test results with CFD (Computational Fluid Dynamics) analysis. Effects of the aeroelastic deformation and the boundary layer transition data of flight test were taken into account to improve CFD analysis.

Fig.1 Scene of the flight test

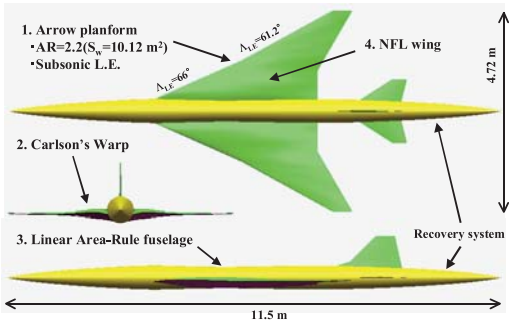

Fig.2 Schematics of the unmanned scaled supersonic experimental airplane (NEXST-1)

2. Background

Figure 3 shows the flight test plan on the NEXST-1 program. The experimental airplane was launched using a rocket booster, and accelerated to M_{inf}=2.1 at 18km altitude. The airplane was separated from the rocket, and started to glide through aerodynamic measurement phases, so called "angle of attack sweep" and "Reynolds Number sweep". After the measurement phases, the airplane reduced its flight speed and descended the altitude, and finally touched down to the ground using a parachute and air bags. The aerodynamic data have been measured, and the experimental airplane have been recovered safely. During the flight test, three types of aerodynamic data, 1) surface pressure distribution, 2) boundary layer transition, 3) aerodynamic forces, were obtained to validate the design concepts.

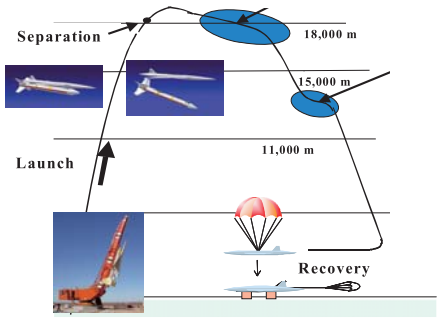

Fig.3 Flight test plan of the NEXST-1 program

3. CFD codes

In this study, two kinds of CFD codes, structured mesh code UPACS and unstructured mesh code TAS, were used. UPACS (Unified Platform for Aerospace Computation Simulation)[6] was the structured mesh code and developed by JAXA, and it is a standard CFD code in Institute of Aerospace Technology of JAXA. The Navier-Stokes flow solver of UPACS is based on a cell-centered finite volume method. The convection terms are discretized using Roe's flux difference splitting with MUSCL extrapolation and no limiter in the present computation. MFGS (Matrix Free Gauss-Seidel) implicit method is used for time integration.

TAS (Tohoku university Aerodynamic Simulation)[7] code including the unstructured mesh generator and flow solver was the unstructured mesh code and developed by Tohoku university and improved by JAXA. It can generate triangular surface mesh with the advancing front method, tetrahedral volume mesh by the method of Delauny tetrahedral meshing as well as hybrid volume mesh composed of tetrahedrons, prisms, and pyramids for viscous flow with high Reynolds number. In TAS code, Navier-Stokes equations are solved on the unstructured mesh by a cell-vertex finite volume method. HLLEW (Harten-Lax-van Lee-Einfeld -Wada) method is used for the numerical flux computations. The second-order spatial accuracy is obtained by a linear reconstruction of the primitive variable. LU-SGS (Lower/Upper Symmetric Gauss-Seidel) implicit method is used for the time integration.

The Splart-Allmaras one equation model[8] is used to simulate turbulent flow in the both codes.

4. Wind tunnel test and CFD validation

Before CFD analysis was performed on the flight test condition, CFD codes was verified using the wind tunnel test results which was performed in a JAXA's 1m×1m supersonic wind tunnel. The measured aerodynamic forces and the surface pressure distributions were obtained on an 8.5% scaled model of NEXST-1 airplane in the wind tunnel test, as shown Figure 4. There are two wind tunnel models. One is called "clean shape", the other is called "additional shape". The additional shape has some additional parts, a pitot prove (ADS), TAT sensor (total temperature sensor), monitor camera (CAMERA) and the hall of joint to the rocket (HALL), as shown Figure 5. The additional shape consists of installing the four additional parts (ADS, TAT, CAMERA and HALL) in the clean shape. Thus, the additional shape has very complex shape to solve for the CFD analysis using the structured mesh code UPACS. Therefore, the CFD analysis using the UPACS was mainly performed on the clean shape. The effects due to the additional parts were estimated using the TAS analysis, because the TAS code using the unstructured mesh can solve the complex shape as the additional shape.

Figure 6 shows the comparison of force data of the wind tunnel test with that of the CFD for the clean shape. And Figure 7 shows the surface C_p (pressure coefficient) distribution of wing surface of the CFD and the Wind tunnel test on four cross sections. First, concerning differences of CFD codes, there are good agreement of C_L, C_D (drag coefficient), C_m (pitching moment coefficient) and C_p distributions between UPACS and TAS. It indicates that the difference between the two CFD

codes is very small. Next, it was investigated that the comparison between results of the wind tunnel test and the CFD (Fig6, Fig7). The relatively agreements in C_L, C_D, C_m were observed on both results. 4cts (drag counts) of C_{Dmin} difference are seen in both results. However, C_p distribution by the CFD are corresponded to the wind tunnel test results. By comparing of the wind tunnel test, the CFD codes could be verified by corresponding with the wind tunnel test results.

Fig.4 8.5% scaled model in wind tunnel test

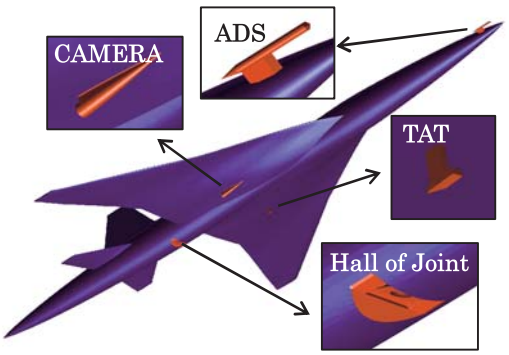

Fig.5 Configuration of Additional parts on the airplane

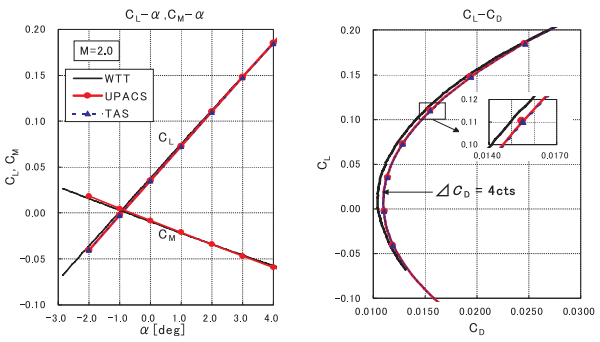

Fig.6 Comparison of the force data between the wind tunnel test and CFD

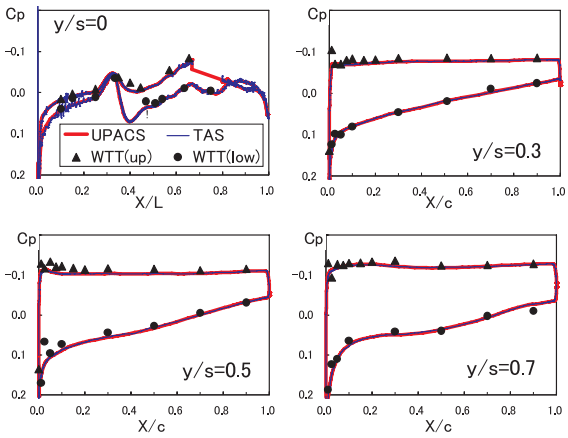

Fig.7 Comparison of C_p distributions between the wind tunnel test and CFD

Next step, effects by the additional parts were cleared by the wind tunnel tests and the CFD analysis using TAS code, which based on an unstructured mesh. Figure 8 shows force data of the wind tunnel test and the CFD result. The differences were not observed for the C_L, C_m. characteristic on the both results. However, the additional parts increase 5.8cts of the drag component on the wind tunnel test result. This 5.8 counts of drag component can be divided to each effects induced by each additional parts. 2.0cts of C_D increment is induced by the ADS. TAT increases 2.5cts of C_D, CAMERA increases 0.7cts and HALL of joint increases 0.6cts of drag component. This fact indicated that the TAT and the ADS has more impact on the drag coefficient than others. 8.3cts of C_D increment of the additional parts was also estimated by the unstructured CFD code TAS. This C_D increment from 5cts to 8cts can be considered to be dependence on the pressure drag, because the increment of the surface area of the additional parts is 0.3% which corresponds to 0.2 friction drag counts. Therefore this C_D increment from 5cts to 8cts should be also considered the drag component of the CFD analysis in the clean shape on the flight test condition. Furthermore, the influence by ADS to the downstream was

investigated. Figure 9 shows comparison of C_p distributions of on the body and the wing surface of the NEXST-1 with ADS and without ADS. It was found that the ADS did not affect downstream C_p distributions. From what has been investigated above, it was cleared that the additional parts are sensitive to drag coefficient C_D, but insensitive to C_L, C_m and C_p distribution on the wing.

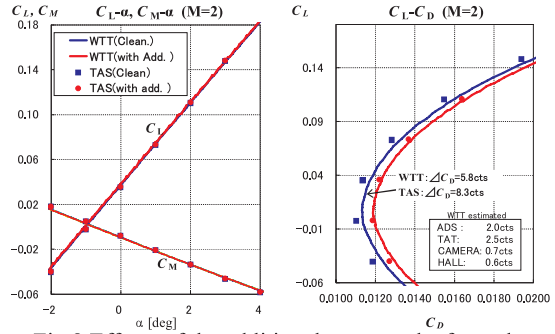

Fig.8 Effects of the additional parts on the force data

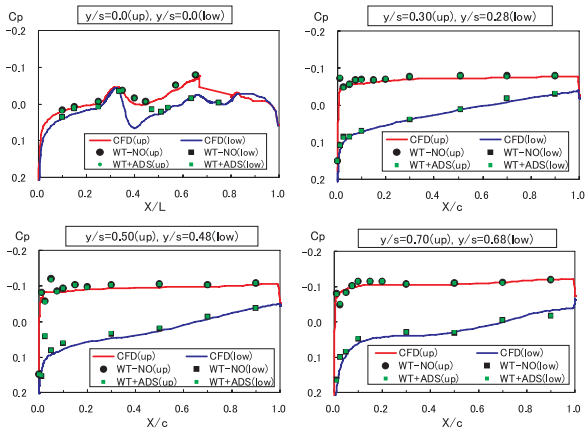

Fig.9 Effects of ADS on Cp distributions

5. Flight test results and CFD validation

a) Measurement phases

After the validation of the CFD codes and the estimation of additional parts effect, The CFD results were compared with the flight test results to verify the design concepts of the NEXST-1. There are two aerodynamic measurement phases near H=18km and 12km at M=2.0 during the flight test, as shown Figure 10. The first one is called "α-sweep", and the other one is called "Re-sweep". Table 1 shows the flight conditions on the each steps of the aerodynamic measurement. Here, the fourth step of the α-sweep is near the design point of the NEXST-1.

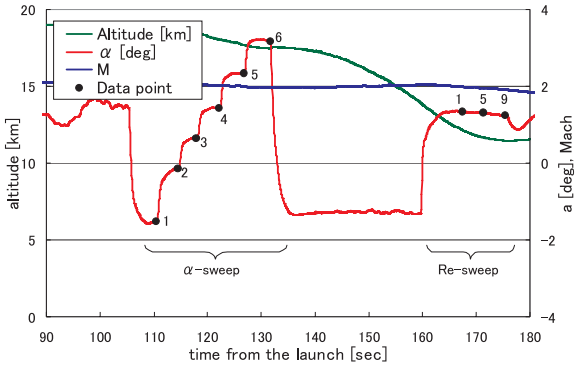

Fig.10 The measurement phase of the NEXST-1 airplane

Table.1 The flight test conditions

Phase	Altitude[km]	Mach	AOA[deg]
αsweep-1	18.917	1.9999	-1.51561
αsweep-2	18.775	2.0166	-0.08762
αsweep-3	18.440	2.0309	0.76661
αsweep-4	18.039	2.0206	1.58843
αsweep-5	17.677	1.9980	2.53952
αsweep-6	17.468	1.9682	3.45185
Re sweep-5	11.646	1.9491	1.68338

b) Effect of the additional parts

At first, the influence of the additional parts at the condition of the flight test was investigated like as the wind tunnel test. Figure 11 shows the surface C_p distribution by the unstructured CFD results on the airplane with the additional parts. Figure 12 shows C_p distributions at four cross sections obtained by the CFD analysis and the flight. With additional parts, it is observed that the C_p distributions were not changed globally, though they were changed only locally in the circled areas in Figure 12. Figure 13 shows in C_L, C_D, and C_m characteristics on the NEXST-1 obtained by the flight test and the CFD analysis. It is also found that 8cts of C_D increases due to additional parts as well as the wind tunnel test. In other words, the CFD and the wind tunnel test results for the additional parts indicated that 5cts-8cts in the drag coefficient should be excluded in that of the CFD for the clean shape.

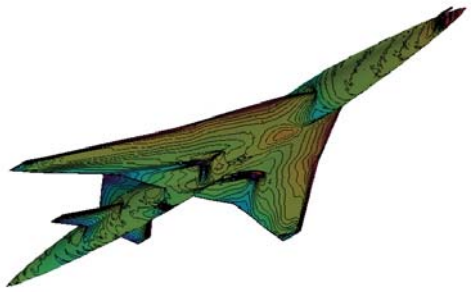

Fig.11 The surface Cp distribution on the airplane with additional parts(α-sweep 4)

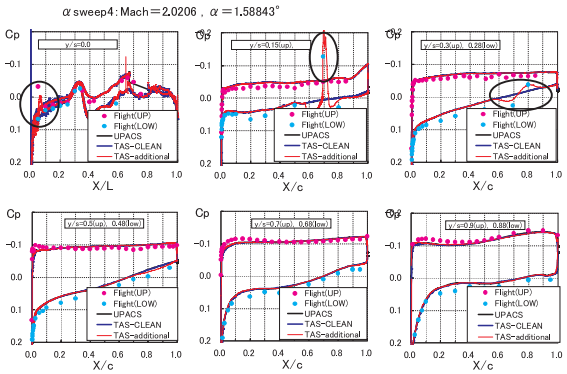

Fig.12 Effects of the additional parts on Cp distributions at the flight condition

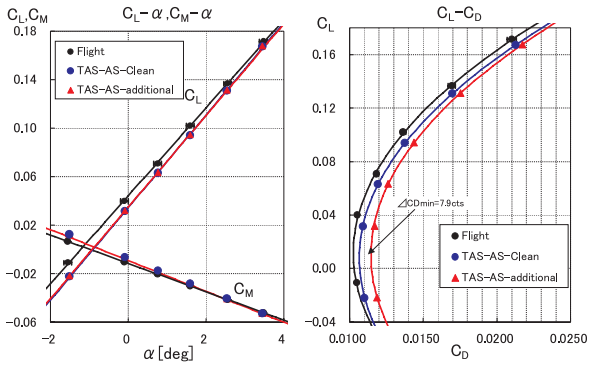

Fig.13 Effects of the additional parts on the force data at the flight condition

c) Method of the CFD analysis

Then, the flight test and the CFD analysis were compared in detail. Efforts are made to improve the accurate of the CFD analysis of the flight test condition. The first is the effect of aeroelastic deformation of the NEXST-1 airplane during the flight test. The other one is the effect of the boundary layer transition on the wing upper surface. They are very important because these are different from the wind tunnel test condition. In this study, the CFD analysis is divided into three types, “AS”, ”ES” and “TR”, as shown table 2. The AS shape is Aerodynamic shape and fully turbulent flow. “ES” means Elastic shape considering the effect of static aeroelastic deformation using NASTRAN and UPACS-“AS”. It is also fully turbulent flow. And “TR” shape is also elastic shape. Further it is combined laminar flow and turbulence flow. Upstream area from the transition line obtained by the flight test were performed laminar flows CFD analysis, on the hand, the downstream area from the transition line were conducted the turbulent flows CFD. Figure 14 shows FEM (Finite Element Method) model of NASTRAN. The ES shape was obtained from using the span load distribution on the AS shape. Figure 15 shows wing section geometry of the elastic shapes (ES). As the angels of attack are increased, the dihedral angle, the twist angle and camber of the wing are changed along the spanwise locations[9]. Figure 16 shows the boundary transition data from the flight test[10,11]. The transition location is specified in the CFD analysis according to the flight test results. The green line is the boundary of non-turbulent and turbulent regions. Type “TR” was performed by the CFD analysis with considering effects of the boundary layer transition. The upstream region of the transition line is set to the laminar flow and the downstream region is the turbulent flow. Transition location moves more downward at the design point then that of the off-design points.

Table.2 CFD analysis types on the flight test

	Shape	Turbulence
AS	Aerodynamic Shape	fully Turbulence
ES	Elastic Shape(wing)	fully Turbulence
TR	Elastic Shape (wing)	Laminar + Turbulence

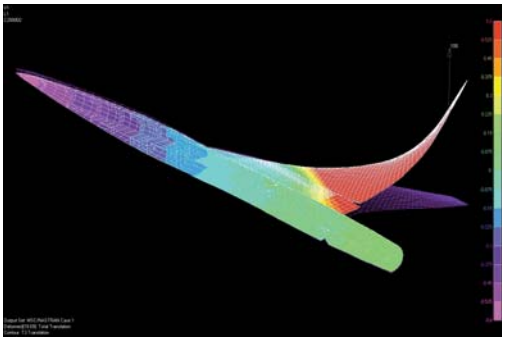

Fig.14 FEM model of NEXST-1

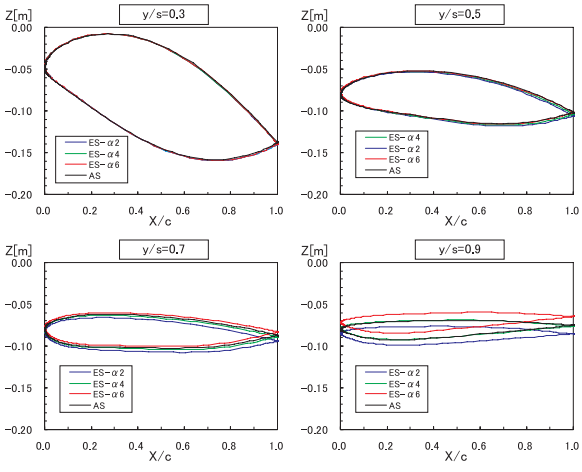

Fig.15 Wing cross section on the aeroelastic shape

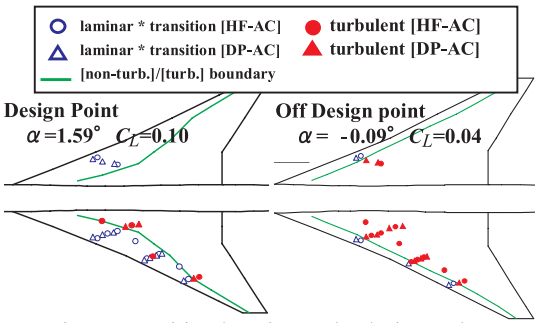

Fig.16 Transition location at the design and off-design condition

d) Results of CFD analysis

Figure17 and Figure 18 show the force data of C_L, C_m and C_D characteristics of the flight test and the CFD analysis. Figure 19 shows the coefficient of the equation, (1) (2) (3) of C_L, C_m and C_D which is approximated by the least square approximation. This figure is useful to understand the effect of the ES and the TR. As Fig17 and Fig18 shown, the UPACS-AS and the TAS-AS also have good agreement in the condition of flight test. Compared with UPACS and the flight test, C_L, C_m of elastic shape is closed to the flight test result. As Figure 19 shown, these closing tendencies is observed not only $C_{L\alpha}$ and $C_{m\alpha}$, but also α_0 and C_{m0}. However, the CFD results are little different with those of the flight test. Figure 18 shows the drag polar curves. Compared with UPACS and the flight test, the transition case influence the C_D and the TR results close to the flight test. Although the C_{Dmin} of "ES" is 4.2cts larger than the flight test result, the C_{Dmin} of "TR" is only 1.0cts larger than the flight test. The decrease of C_{Dmin} results from the reduction of the friction drag due to considering the boundary layer transition. Here, considering the additional parts, it is estimated that the discrepancy of C_{Dmin} of the CFD analysis and the flight test result is from 6cts to 9cts. Figure 21 shows surface C_p at an off-design point and Figure 22 is that at the design point at the several span wise locations. The error-bars on the C_p distributions are the uncertainly of the pressure measurement system mentioned above section (ΔC_p=0.0115). It is observed that the C_p distributions by the wing-tip of "ES" closes to the flight test results. The CFD analysis is almost corresponding to the flight test result, however it is not perfectly corresponding especially at lower and inner surface. This reason has not been well understood, so it calls for further investigation. However, the discrepancy of the CFD from the flight test becomes small at the design point, and a good agreement for the CFD with the flight test is obtained except inner wing.

$$C_L = C_{L\alpha}[\alpha - \alpha_0] \quad (1)$$

$$C_D = K(C_L - C_{L0})^2 + C_{D,min} \quad (2)$$

$$C_m = C_{m\alpha} \cdot \alpha + C_{m0} \quad (3)$$

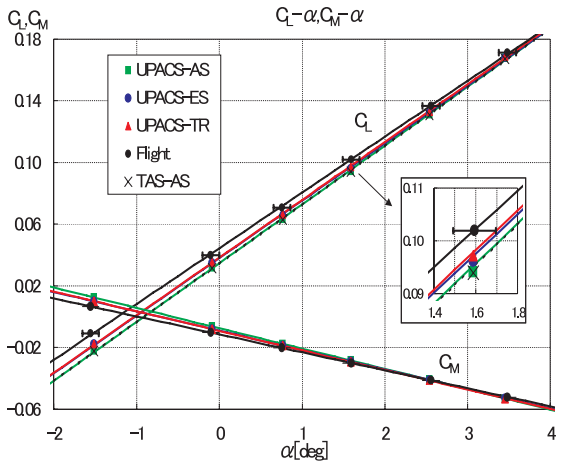

Fig.17 C_L and $C_m$characteristic on "a-sweep" test phase

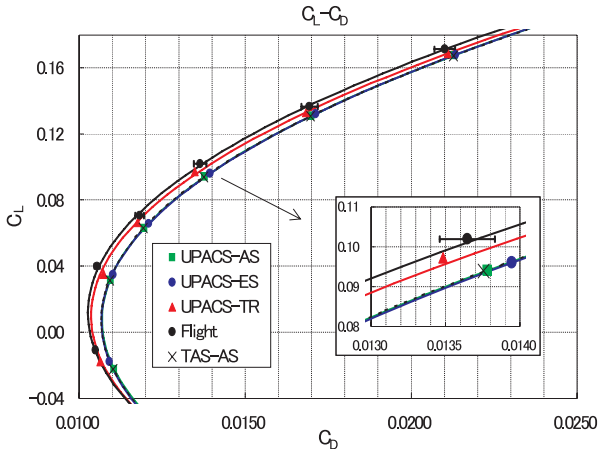

Fig.18 Drag polar on "a-sweep" test phase

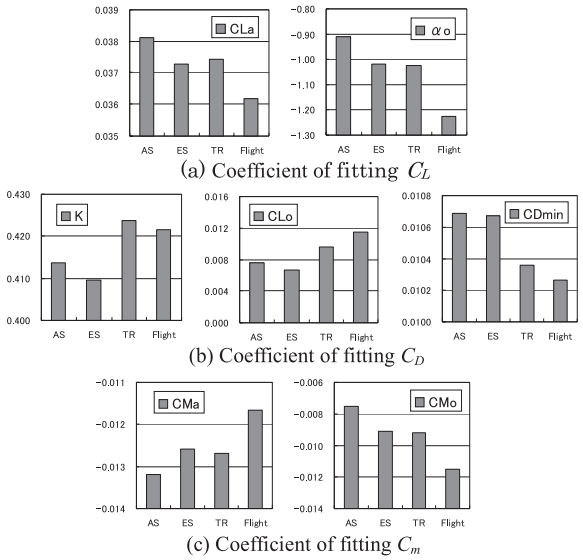

(a) Coefficient of fitting C_L

(b) Coefficient of fitting C_D

(c) Coefficient of fitting C_m

Fig.19 Coefficient of fitting C_L, C_D and C_m

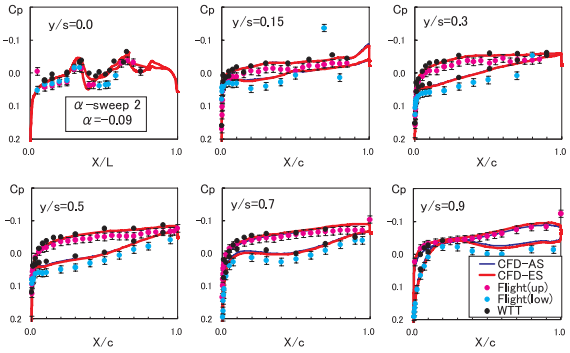

Fig.20 C_p distribution at the off-design point

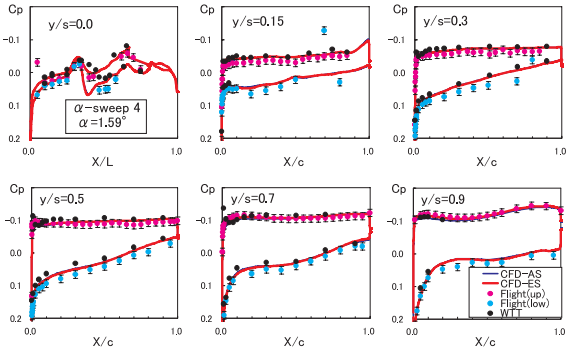

Fig.21 C_p distribution at the design point

e) Effect of natural laminar flow wing

From above the investigations, the effect of the natural laminar flow wing which is one of the most important design concepts of the NEXST-1, was estimated from the Flight test and the CFD analysis. Figure 22 shows C_D at variable angles of attack. The ΔC_D is the difference of C_D between the ES and the TR. When the ΔC_D is larger, it is meant that the drag component of the NEXST-1 including the results about the boundary layer transition decreases by the effect of the natural laminar flow wing design concept. It is found the effect is the highest at the design point (α-sweep 4, α=1.59deg), and the C_D is 4.6cts lower than that of the fully turbulent flow. This 4.6cts reduction indicates the effect of the natural laminar flow wing design concept. It is cleared that the natural laminar flow wing design concept of the NEXST-1 was effective at the condition of flight test.

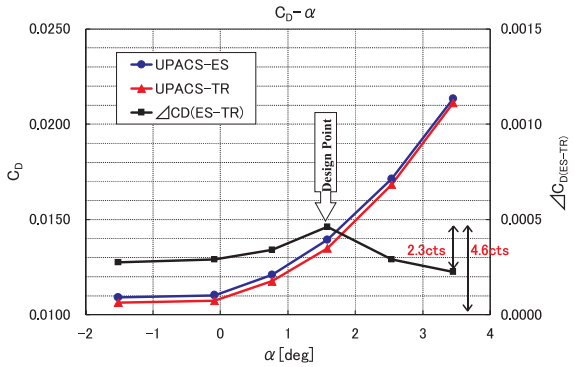

Fig.22 Effect of Natural Laminar Flow wing

6. Conclusions

The CFD analysis of NEXST-1 was performed to verify the design concept of the NEXST-1 using two CFD codes, structured mesh code UPACS and unstructured mesh code TAS. Before computation about the flight test condition, the validation of their CFD codes and the effect of the additional parts was estimated by the wind tunnel test. After the validation of the CFD code and the estimation of additional parts effect, the CFD analysis was compared with the flight test results. Effects of aeroelastic deformation and the boundary layer transition data of flight test were taken into account to improve CFD analysis. And it was shown that the effect of aeroelastic deformation improves C_L, C_m and C_p distribution, and the effect of the boundary layer transition improves C_D. The CFD analysis is almost corresponding to the flight test result, the reason of the discrepancy is not clear, so further investigation is required. Finally, the effect of the natural laminar flow wing was assessment. It is found that the effect is the highest at the design point (α-sweep 4, α=1.59deg), and the C_D is 4.6cts lower than that of the fully turbulent flow. It is confirmed that the concepts of natural laminar flow wing design using the NEXST-1 was effective at the condition of flight test.

7. References

1. Sakata,K,. “Supersonic Experimental Airplane (NEXST-1) for Generation SST Technology -Development and Flight Test Plan for the Unmanned Scaled Supersonic Glider-,“ AIAA Paper 2002-0527, Reno, Jan. 2002
2. Ohnuki, T., Hirako, K., and Sakata, K., “National Experimental Supersonic Transport Project,” *International Congress of the Aeronautical Science,* 2006-1.4.1,.
3. Kwak,D,. Yoshida,K, Ishikawa,K and Noguchi,M., “Flight Test Measurements of Surface Pressure on Unmanned Scaled Supersonic Experimental Airplane,” AIAA Paper2006, 2006.
4. Yoshida,K,. and Makino,Y., “Aerodynamic Design of Unmanned and Scaled Supersonic Experimental Airplane in Japan,” *ECOMAS 2004*, Finland, Jul. 2004.
5. Ishikawa,H,. Kuroda,F and Yoshida,K., “Study on Supersonic Drag Reduction Concept of SST -Comparison of Linear Theory and CFD Analsis-,” *35th JAPAN Society for Aeronautical and Space Science Annual Conference*, Mar. 2004. (in Japanese)
6. Takaki,R., Yamamoto,K. Ymane,T. Enomoto,S and Mukai,J., “The Development of the UPACS CFD Environment,” *High Performance Computing, Proc. of ISHPC 2003*, Springer, pp.307-319, 2003
7. Nakahashi,K., Togashi,F., Fujita,T. and Ito,Y., “Numerical Simulations on Separation of Scaled Supersonic Experimental Airplane from Rocket Booster at Supersonic Speed,” AIAA Paper 2002-2843,2002
8. Spalart,P.R. and Allmaras,S.R., “A One-Equation Turbulence Model for Aerodynamic Flow,” AIAA Paper 92-0439, 1992.
9. Kawakami,H,. Kurotaki,T., Takatoya,T., Ueda,Y and Kuroda,F., “Aeroelastic Analysis of the Non-powered Supersonic Experimental Airplane”, *41st Aircraft Symposium*, Nagano, Oct. 2003 (in Jpanese)
10. Yoshida,K., Kwak,D.Y, Tokugawa,N. and Makino,Y., “Supersonic Experimental Airplane (NEXST-1) -Aerodynamics and Measurement System Design-,” *37th Japan Society for Aeronautical and Space Science Annual Conference*, Mar. 2006. (in Japanese)
11. Tokugawa,N., and Yoshida,K., “Transition Detection on Supersonic Natural Laminar Flow Wing in the Flight,” AIAA Paper2006-3165, 2006